Nuclear Instruments and Methods in Physics Research A 765 (2014) 161–166

Contents lists available at ScienceDirect

Nuclear Instruments and Methods in Physics Research A

journal homepage: www.elsevier.com/locate/nima

Investigation of silicon sensors for their use as antiproton annihilation detectors

N. Pacifico [a,*], S. Aghion [b,c], O. Ahlén [d], A.S. Belov [e], G. Bonomi [f,g], P. Bräunig [h], J. Bremer [d], R.S. Brusa [i,j], G. Burghart [d], L. Cabaret [k], M. Caccia [l], C. Canali [m], R. Caravita [n,o], F. Castelli [p], G. Cerchiari [q], S. Cialdi [p], D. Comparat [k], G. Consolati [b,c], C. Da Via [r], J.H. Derking [d], S. Di Domizio [n,o], L. Di Noto [o], M. Doser [d], A. Dudarev [d], R. Ferragut [b,c], A. Fontana [g], P. Genova [g], M. Giammarchi [c], A. Gligorova [a], S.N. Gninenko [e], S. Haider [d], J. Harasimowicz [s], T. Huse [t], E. Jordan [q], L.V. Jørgensen [d], T. Kaltenbacher [d], A. Kellerbauer [q], A. Knecht [d], D. Krasnický [n], V. Lagomarsino [n], S. Lehner [u], A. Magnani [g,v], C. Malbrunot [u], S. Mariazzi [u], V.A. Matveev [e,w], F. Moia [b,c], G. Nebbia [x], C. Nellist [r], P. Nédélec [y], M.K. Oberthaler [h], V. Petráček [z], F. Prelz [c], M. Prevedelli [aa], C. Regenfus [m], C. Riccardi [g,v], O. Røhne [t], A. Rotondi [g,v], H. Sandaker [a], A. Sosa [s], M.A. Subieta Vasquez [f,g], M. Špaček [z], G. Testera [n], C.P. Welsch [s], E. Widmann [u], P. Yzombard [k], S. Zavatarelli [n], J. Zmeskal [u]

[a] University of Bergen, Institute of Physics and Technology, Allégaten 55, 5007 Bergen, Norway
[b] Politecnico di Milano, Piazza Leonardo da Vinci 32, 20133 Milano, Italy
[c] Istituto Nazionale di Fisica Nucleare, Sez. di Milano, Via Celoria 16, 20133 Milano, Italy
[d] European Organisation for Nuclear Research, Physics Department, 1211 Geneva 23, Switzerland
[e] Institute for Nuclear Research of the Russian Academy of Sciences, Moscow 117312, Russia
[f] University of Brescia, Department of Mechanical and Industrial Engineering, Via Branze 38, 25133 Brescia, Italy
[g] Istituto Nazionale di Fisica Nucleare, Sez. di Pavia, Via Agostino Bassi 6, 27100 Pavia, Italy
[h] Kirchhoff Institute for Physics, Im Neuenheimer Feld 227, 69120 Heidelberg, Germany
[i] Department of Physics, University of Trento, via Sommarive 14, 38123 Povo, Trento, Italy
[j] INFN-TIFPA, via Sommarive 14, 38123 Povo, Trento, Italy
[k] Laboratoire Aimé Cotton, CNRS, Université Paris Sud, ENS Cachan, Bâtiment 505, Campus d'Orsay, 91405 Orsay Cedex, France
[l] University of Insubria, Dipartimento di Scienza ed Alta Tecnologia, via Valleggio 11, Como, Italy
[m] University of Zurich, Physics Institute, Winterthurerstrasse 190, 8057 Zurich, Switzerland
[n] Istituto Nazionale di Fisica Nucleare, Sez. di Genova, Via Dodecaneso 33, 16146 Genova, Italy
[o] University of Genoa, Department of Physics, Via Dodecaneso 33, 16146 Genova, Italy
[p] University of Milano, Department of Physics, Via Celoria 16, 20133 Milano, Italy
[q] Max Planck Institute for Nuclear Physics, Saupfercheckweg 1, 69117 Heidelberg, Germany
[r] School of Physics and Astronomy, University of Manchester, Manchester, United Kingdom
[s] University of Liverpool and the Cockroft Institute, Liverpool, Sci-Tech Daresbury, Keckwick Lane, Daresbury, Warrington WA4 4AD, United Kindom
[t] University of Oslo, Department of Physics, Sem Sælandsvei 24, 0371 Oslo, Norwayy
[u] Stefan Meyer Institute for Subatomic Physics, Austrian Academy of Sciences, Boltzmanngasse 3, 1090 Vienna, Austria
[v] University of Pavia, Department of Nuclear and Theoretical Physics, Via Bassi 6, 27100 Pavia, Italy
[w] Joint Institute for Nuclear Research, 141980 Dubna, Russia
[x] Istituto Nazionale di Fisica Nucleare, Sez. di Padova, Via Marzolo 8, 35131 Padova, Italy
[y] Claude Bernard University Lyon 1, Institut de Physique Nucléaire de Lyon, 4 Rue Enrico Fermi, 69622 Villeurbanne, France
[z] Czech Technical University in Prague, FNSPE, Břehová 7, 11519 Praha 1, Czech Republic
[aa] University of Bologna, Department of Physics, Via Irnerio 46, 40126 Bologna, Italy

ARTICLE INFO

Available online 19 June 2014

Keywords:
Silicon
Antiprotons
Detector

ABSTRACT

We present here a new application of silicon sensors aimed at the direct detection of antinucleons annihilations taking place inside the sensor's volume. Such detectors are interesting particularly for the measurement of antimatter properties and will be used as part of the gravity measurement module in the AEgIS experiment at the CERN Antiproton Decelerator. One of the goals of the AEgIS experiment is to measure the gravitational acceleration of antihydrogen with 1% precision. Three different silicon sensor

* Corresponding author.
E-mail address: nicola.pacifico@cern.ch (N. Pacifico).

http://dx.doi.org/10.1016/j.nima.2014.06.036
0168-9002/

AEgIS
Strip
Pixel

geometries have been tested with an antiproton beam to investigate their properties as annihilation detection devices: strip planar, 3D pixels and monolithic pixel planar. In all cases we were successfully detecting annihilations taking place in the sensor and we were able to make a first characterization of the clusters and tracks.

1. Introduction

The goal of the AEgIS experiment [1] located at the CERN Antiproton Decelerator (AD) [2] is to make the first measurement of the acceleration of antimatter in the Earth's gravitational field. AEgIS will also be the first experiment to use a segmented silicon sensor as part of a hybrid position sensitive detector, the *Gravity Module*, to directly detect the annihilation position of cold antihydrogen atoms. After the production and acceleration of a pulsed beam of antihydrogen atoms upstream in the apparatus (100 mK), the antihydrogen atoms pass through a moiré deflectometer [3] producing a fringe pattern on the annihilation plane: the segmented silicon detector (see Fig. 1) provides TOF information and a first position resolution of ~7–8 μm. The annihilation products will travel on and leave tracks in the emulsion detector [4] that will provide high resolution (1–2 μm) position reconstruction. A scintillating fiber tracker located behind the emulsion detector (not shown in Fig. 1) will also provide 3D online information on the antihydrogen annihilation vertex and on the TOF. Together this hybrid position detector will achieve a resolution of 1% on the gravitational acceleration of antihydrogen with 600 events [4].

This is the first adaptation of a silicon detector for direct measurement of antimatter annihilation. Previous works [5] report the use of silicon as an active annihilation target, but no position resolution was provided in that case. We present new results on the annihilation detection capabilities of three different types of silicon detectors:

- planar strip;
- 3D pixels;
- monolithic planar pixel.

The analysis and the comparison of the results obtained with the different geometries will be presented in Section 4.

2. Silicon as an annihilation detector

When antihydrogen approaches matter, the positron annihilates with an electron, generating 2 × 511 keV photons – towards which silicon tracking sensors have no sensitivity. For this reason, once ensured , the annihilation of antiprotons can be deemed to be equivalent to annihilation of antihydrogen atoms. The distinction between antihydrogen and antiprotons has to be ensured independently (in our case through discrimination of the flight times).

When an antiproton annihilates with a nucleon from a silicon atom, the primary products of annihilation are the charged and neutral pions. Charged pions are emitted with an average multiplicity of 1.53 ± 0.03 pions per charge sign [6]. One of the pions can interact with the nucleus, fragmenting it. Fragments are then emitted with kinetic energies in the order of tens to hundreds of MeV [6]. Detection of primary charged pions and of charged fragments can be used as a signature of an annihilation event. Detectable annihilation products can be emitted within a wide range of multiplicities and kinetic energies [6]. The upper limit for the kinetic energy of annihilation products is set by the total energy released by the annihilation of a nucleon and an antinucleon (~1880 MeV). Some of the products (protons, pions) can have a travel range in excess of several millimeters, resulting in the production of charge clusters which can spread as well over several millimeters. A proper understanding of the annihilation signature is thus necessary in order to identify the real annihilation point.

We performed Geant4 simulations on single annihilation events in silicon, using the Fritjof-Precompound physics list as included in Geant4 (version 4.9.5) [7]. Fig. 2 shows the simulated distribution of the most important annihilation products in silicon. Among the charged products, keeping in mind the maximum total energy released in an annihilation event, one can predict (for example using a tool like SRIM [8]) that heavy nuclear fragments will be responsible for high and localized energy depositions. Lighter fragments and pions, with longer stopping ranges, are able

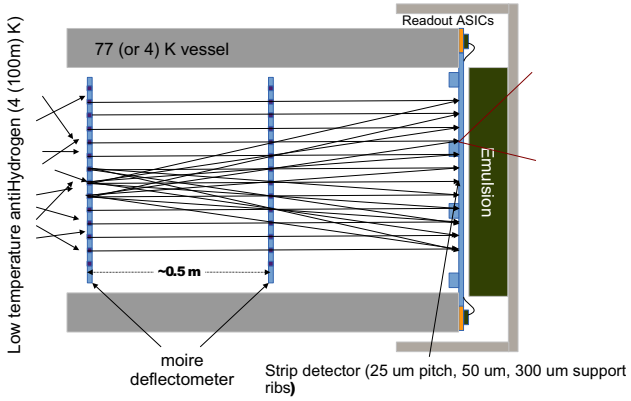

Fig. 1. The gravitational measurement with the *Gravity Module*, as proposed in AEgIS: A moiré deflectometer produces a fringe pattern on the silicon detector where the antihydrogen atoms annihilate. Behind there is a high resolution emulsion detector for reconstruction of the annihilation products.

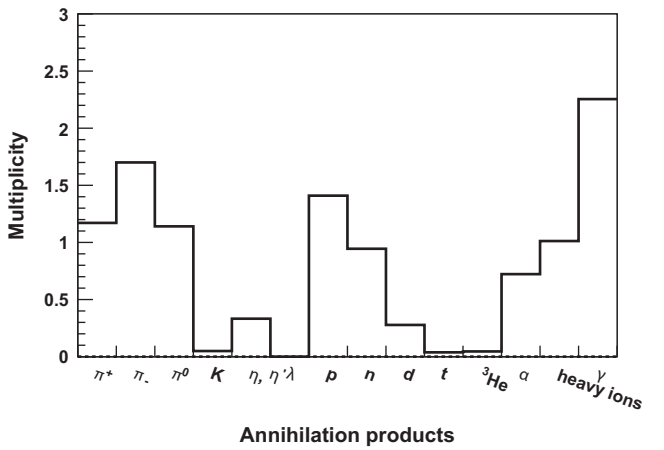

Fig. 2. Average multiplicity of the different products for the annihilation of a single antiproton on a silicon atom as simulated in Geant4 with the Fritjof-Precompound physics list.

to produce longer tracks, inducing signal on a larger number of electrodes, depending on the electrodes' geometry.

3. Test beam setup and facility

The work presented here is the result of two test-beam campaigns in 2012. The AD delivers slow antiprotons to different experiments: the antiprotons are delivered in bunches of $\sim 10^7$ antiprotons spaced by 100 s each. The beam is practically monochromatic, with a kinetic energy of 5.3 MeV. Antiprotons were further slowed down in the AE$\bar{g}$IS apparatus by means of aluminum and silicon degrading foils. The average kinetic energy of the antiprotons impinging on the silicon sensor was of $\sim$100 keV. We performed Geant4 simulations showing that at this kinetic energy practically all the antiprotons are stopped within 14 μm of silicon, which is the smallest thickness among the sensors studied in this work.

A solenoidal magnetic field, with an intensity up to 5 T, was used to keep the antiprotons collimated within the apparatus. A vacuum chamber was placed in the downstream (diverging) fringe field of the magnet. In the vacuum chamber the different sensors under study were installed. All the readout systems used in the present work were triggered with a digital signal provided by the AD and coincident with the beam.

3.1. Planar strip sensors

Planar strip sensors are the geometry to be adopted in the construction of AE$\bar{g}$IS annihilation plane. Among the advantages of planar strip sensors specific to our application we can list the following:

- Possibility to have a very thin sensing region while keeping the readout electronics mounted on the edges, thus not contributing to the total thickness of the sensor, minimizing the material budget on the path of annihilation products.
- Possibility to operate the detector cold: the thermal management of the ASICs can be handled separately from the sensor's bulk.

The two planar strip sensors tested here were manufactured by Helsinki Institute of Physics (HIP) on standard 300 μm thick, MCz n-type wafers. Strips were realized as p^+ implants, with AC coupled aluminum readout strips. Of the two sensors, one had 50 μm strip pitch, and the other one 80 μm. The strip length was of 1 cm.

The sensors were read out through the Alibava system [9], employing two Beetle chips, used in the LHCb Velo readout system. These chips provided, in our configuration, a dynamic range spreading from $\sim$20 (5 noise RMS) up to 800 keV, where signal saturation occurred. For the purposes of this work, the calibration (occurred charge / ADC) was performed with the calibration capacitor built into the Alibava system, up to the observed channel saturation.

Depletion voltage of the silicon sensors was measured with standard CV characterization, with a full depletion voltage of $\sim$120 V. *IV* characterization showed a breakdown voltage $>$300 V. The maximum applied voltage throughout this study was 150 V.

3.2. 3D pixel sensor

The 3D pixel sensors studied in this work were manufactured by CNM (Barcelona) as prototypes for the ATLAS Insertable B-layer (IBL) [10]. Sensor thickness was 230 μm. Pixels were arranged in a 80 $\times$ 336 matrix, forming a square with a side of 2 cm. Pixel size was 50 $\times$ 250 μm^2. These sensors were overlaid by a composite passivation layer (1.5 μm Al + 0.8 μm doped polysilicon and 1.150 μm of thermal oxide). The sensors were ball-bonded to the FE-I4 readout chip, also developed for the ATLAS IBL. The readout system was the USBPix [11]. The sensors had a nominal depletion voltage of 15 V, and were biased at 30 V throughout the measurements.

3.3. Monolithic planar pixel sensor

We include in the present work, for comparison purposes, data obtained previously using a monolithic active pixel sensor (MAPS), the MIMOTERA [12], developed for hadron therapy monitoring application. A detailed study on the performances of this sensor in antiproton detection is being published separately. The MIMOTERA is a thin diffusion sensor with an active thickness of 14 μm. The readout is divided into a matrix of 112 $\times$ 112 square pixels, 153 μm in side. One of the most important characteristics of the MIMOTERA, exploited in the present study, is its high dynamic range: while almost blind to transversal MIPS, the MIMOTERA is able to resolve events with a high energy deposition, up to $\sim$30 MeV per pixel.

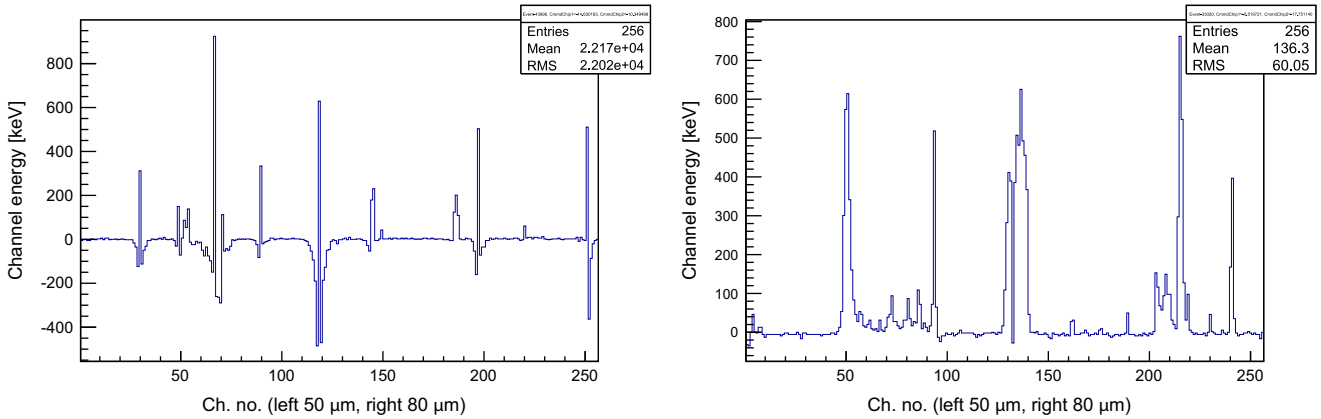

Fig. 3. Sample frames for the planar strip sensor at 2 different voltages. Left: 0.6 V. Right: 150 V. For both histograms, the first 128 channels show data from the 50 μm pitch sensor, channels from 129 to 256 refer to the sensor with 80 μm pitch. The undershoot observed at the lowest voltage is to be ascribed to the high interstrip capacitance for heavily underdepleted sensors.

4. Data analysis and comparisons

Both the planar strip and the 3D pixel sensors were tested throughout December 2012 beamtime at the AEgIS facility. Data with the planar strip sensors was acquired at different bias voltages, namely 0.6 V (∼ built-in potential), 2.2 V, 5 V and 150 V (overdepleted) to study the effect of the active thickness on the acquired signal. The three lower bias voltages correspond to a depleted thickness of 20 μm, 40 μm and 60 μm. Sample frames are shown in Fig. 3 for the lowest and the highest applied bias (0.6 and 150 V).

In an effort to distinguish between different annihilation events, charge clustering was performed by searching for sets of neighboring strips with each strip having a charge higher than 5 noise RMS. At lower bias voltages the typical annihilation event is characterized by very narrow (1–2 strips) clusters, in both sensors with 50 and 80 μm pitch. Neighboring strips often exhibit a negative charge signal. Since, as we will see, this behavior is not observed at higher bias voltages, it is very likely to be ascribed to the strong interstrip capacitance appearing at lower bias, which causes the induction of big charges of opposite sign on the closest neighbors to the fired strips. Increasing the bias voltage at 5 V already reduces the magnitude of this effect that disappears completely at full depletion. Furthermore, higher bias voltages increase the average cluster size. Most of the events are fairly energetic (>200 keV, up to saturation). The high energy deposited (compared to the reduced depleted volume) and the extremely localized charge deposition hint to a signal produced by high Z nuclear fragments, in which the stopping range in silicon can be as short as few μm [8].

Figs. 5 and 6 show the distribution of cluster size and cluster energy for two of the highest and lowest bias voltages applied respectively. The results for 50 and 80 μm pitch were compatible within error bars, hence the shown distributions cumulate the two data sets for the two strip pitches. An increase in the cluster size is observed with higher bias voltages. Almost 80% of the clusters are formed by either 1 or 2 strips at the lowest applied bias. The cluster size increases with voltage, as expected, as the sensors become sensitive to long-range particles (pions and high energy protons) which can travel at an angle within the sensor's volume. The cluster energy spectrum is also affected by the different sensitivities at different voltages: since at low depletion the detector is only sensitive to highly ionizing fragments, the average cluster energy is higher, with most clusters concentrating on energies lower than ∼600 keV.

Data taking with the 3D pixel sensors was carried out using two sensors with equal characteristics. Clusters were defined as conglomerates of fired pixels neighboring in the horizontal, vertical or diagonal direction. A sample frame from the acquisition is shown in Fig. 4. Fig. 7 shows the cluster size distribution while

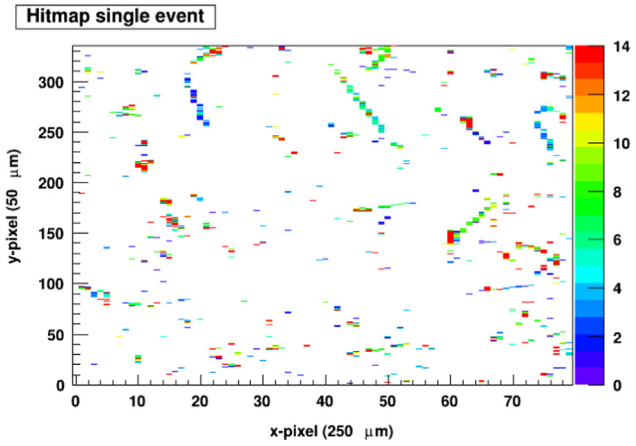

Fig. 4. Sample frame taken with the 3D pixel sensor. Tracks produced from annihilation products travelling in-plane are visible, along with saturated pixels (red) corresponding to large energy deposits by highly ionizing fragments. (For interpretation of the references to color in this figure caption, the reader is referred to the web version of this paper.)

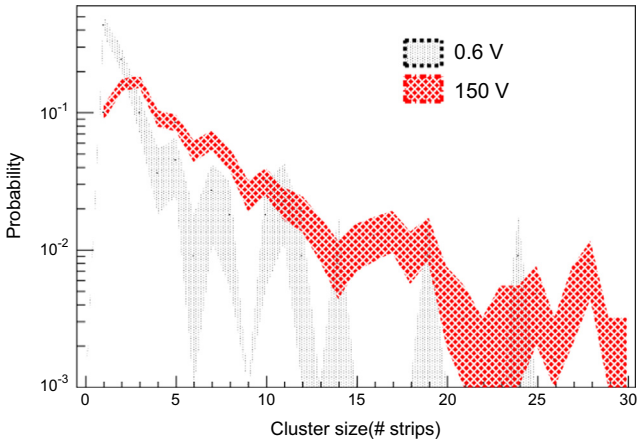

Fig. 5. Cluster size distribution for the planar strip sensor, normalized to unit total integral.

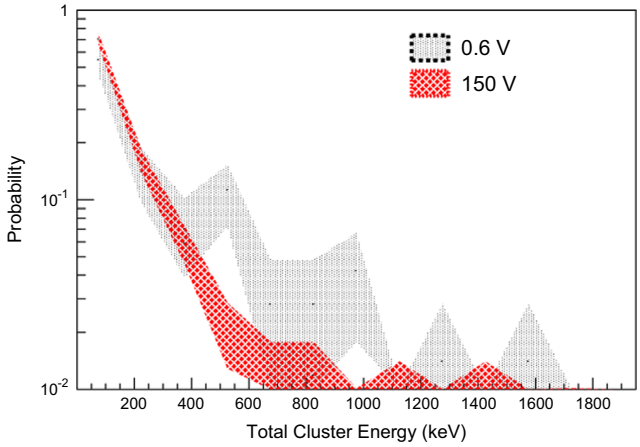

Fig. 6. Deposited energy distribution of the clusters taken with the planar strip sensor, normalized to unit total integral.

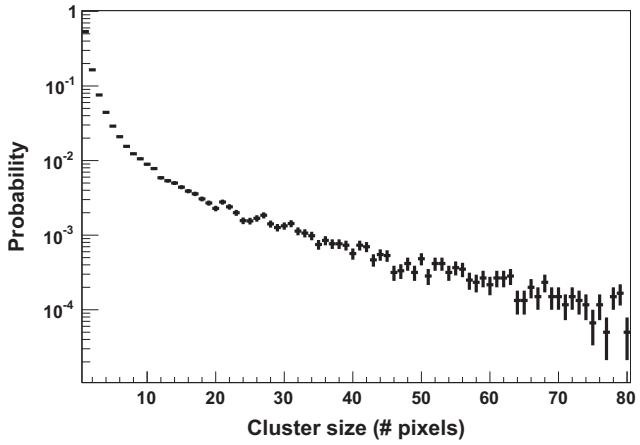

Fig. 7. Cluster size distribution for the 3D pixel sensor, normalized to unit total integral.

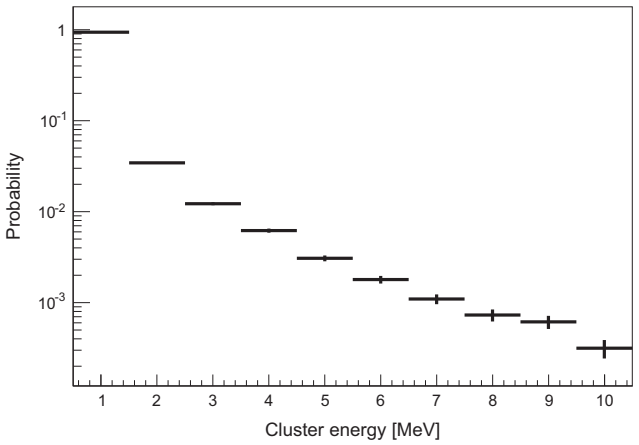

Fig. 8. Deposited energy distribution of the clusters taken with the 3D pixel sensor, normalized to unit total integral.

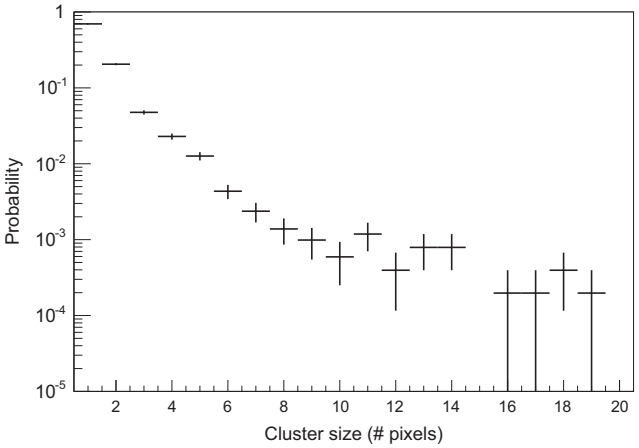

Fig. 9. Cluster size distribution for the monolithic planar pixel sensor, normalized to unit total integral.

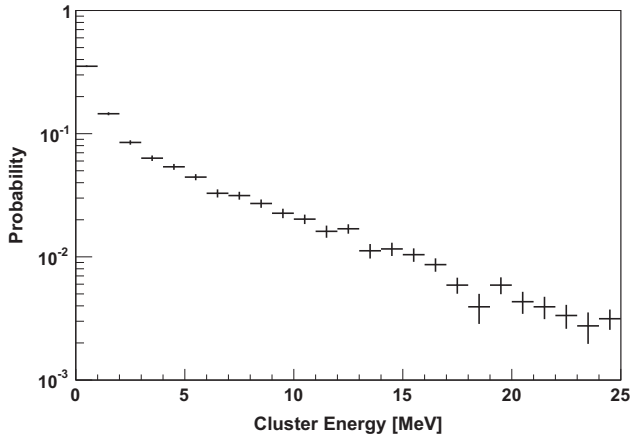

Fig. 10. Deposited energy distribution of the clusters taken with the monolithic planar pixel sensor, normalized to unit total integral.

Fig. 8 shows the cluster energy distribution: more than 90% of the clusters have an energy lower than 400 keV and a size lower than 10 pixels. However, for some clusters, a deposited energy of more than 10 MeV can be observed. One should observe here that, given the relatively low ($\sim$100 keV) saturation limit for the 3D pixel sensor, high values of collected charge are associated with very large clusters. Finally, Figs. 9 and 10 show the distributions for the cluster size and the cluster energy for the monolithic planar pixel sensor respectively. Clustering was done according to the procedure followed for the 3D pixel sensor. The thin active region accounts for relatively small clusters: in order to produce a track of length l, a particle should cross the sensor with an angle equal to $90^\circ + 14\ \mu m/l$. Tracks longer than 1 mm thus constitute $\ll 1\%$ of the total number of tracks. However, due to its design optimized for slow charged hadron detection, no saturation effects were observed. The cluster charge distribution thus accounts for the total energy deposited in the silicon sensor. The obtained results show a strong dependance of the average cluster width from the thickness of the active region and the sensitivity to low ionizing particles – MIPs are visible for example in the depleted silicon strip sensor and the 3D pixel sensor. High ionizing particles (e.g. nuclear fragments) can saturate these devices. Thin sensors on the other hand do not saturate, but their larger dynamic range is normally associated with a decreased sensitivity to MIP particles.

5. Summary and conclusions

We employed three different kinds of silicon particle sensors for detecting slow antiprotons. The aim of the test was to verify the different signatures of an annihilation event in sensors which were designed to detect *minimum ionizing particles* (planar strip and 3D pixel sensors) or slow charged hadrons (planar monolithic pixel sensor). All three kinds of sensors successfully detected antiproton annihilations. The annihilation events were always characterized by large releases of energy. The size of clusters associated with annilation events increased with the thickness of the active volume, as a result of a major sensitivity to annihilation products travelling sideways with respect to the incoming antiprotons.

The presented test-beam data allows us to define requirements for silicon sensors to be used as annihilation detectors. A sensor with a thin active volume produces small clusters, helping localizing spatially the annihilation event through detection of highly ionizing fragments. A readout electronics with a wide dynamic range is moreover to be favored, as signal saturation can easily occur on sensors designed for MIPs.

A planar strip sensor will be installed in the AE$\bar{g}$IS experiment for the detection of annihilation of very slow antihydrogen atoms. The sensor will be physically thin (50 μm) for limited scattering of the annihilation products (to be detected by a downstream emulsion detector). The thin bulk will improve position resolution, while a specific readout ASIC will be able to cope with the wide signal range. Further simulation work, currently in progress, will investigate new reconstruction algorithms to optimally determine the annihilation position with the highest possible resolution.1

Acknowledgments

This work was supported by the Research Council of Norway (project FRINAT no. 213471) and the Bergen Research Foundation (project no. 804390).

We would like to express our thanks to the CERN RD50 group, for providing the Alibava system used for the ministrip measurement. The excellent ministrip sensors were provided by Jaakko Härkönen (Helsinki Institute of Physics), to whom we express our appreciation. We would also like to thank Andrea Micelli and the IFAE (Barcelona), for the support provided with the 3D pixel sensor measurements.

References

[1] A. Kellerbauer, et al., Nuclear Instruments and Methods in Physics Research Section B 266 (3) (2008) 351.

[2] S. Baird, et al., Nuclear Instruments and Methods in Physics Research Section A 391 (1997) 210.
[3] M.K. Oberthaler, et al., Physical Review A 54 (4) (1996).
[4] S. Aghion, Journal of Instrumentation P08013 (2013).
[5] McGaughey, et al., Nuclear Instruments and Methods 249 (1986) 361.
[6] G. Bendiscioli, D. Kharzeev, A Review of Experimental Data (Rivista del Nuovo Cimento) 17 (6) (1994) 1.
[7] ⟨http://geant4.cern.ch⟩.
[8] J.F. Ziegler, et al., SRIM—The Stopping and Range of Ions in Matter, Lulu Press Co., USA, 2008.
[9] R. Marco-Hernandez, Nuclear Instruments and Methods in Physics Research Section A 623 (1) (2010) 207.
[10] Cinzia DaVià, et al., Nuclear Instruments and Methods in Physics Research Section A 699 (2013) 18.
[11] M. Backhaus, et al., Nuclear Instruments and Methods in Physics Research Section A 650 (2011) 37.
[12] R. Boll, et al., Radiation Measurements 46 (12) (2011) 1971.